




ORIGINAL ARTICLE

Experimental validation of a computational fluid dynamics model using micro-particle image velocimetry of the irrigation flow in confluent canals

Mário Rito Pereira¹  | Goncalo Silva² | Viriato Semiao³ | Vania Silverio^{4,5} |
Jorge N. R. Martins¹  | Paula Pascoal-Faria^{6,7} | Nuno Alves⁷ | Juliana R. Dias⁷ |
António Ginjeira¹ 

¹Department of Endodontics, Faculdade de Medicina Dentária, Universidade de Lisboa, Lisbon, Portugal

²IDMEC, Department of Mechatronics, Universidade de Évora, Évora, Portugal

³IDMEC, Departamento de Engenharia Mecânica, Instituto Superior Técnico, Universidade de Lisboa, Lisbon, Portugal

⁴Instituto de Engenharia de Sistemas e Computadores – Microsistemas e Nanotecnologias, INESC MN, Lisbon, Portugal

⁵Department of Physics, Instituto Superior Técnico, Universidade de Lisboa, Lisbon, Portugal

⁶Mathematics Department of the School of Technology and Management (ESTG), Marinha Grande, Portugal

⁷Centre for Rapid and Sustainable Product Development (CDRSP), Instituto Politécnico de Leiria, Marinha Grande, Portugal

Correspondence

Mário Rito Pereira, Faculdade de Medicina Dentária da Universidade de Lisboa, Rua Professora Teresa Ambrósio, Cidade Universitária, 1600-277 Lisboa, Portugal.
Email: mariorp@campus.ul.pt

Funding information

Fundação para a Ciência e a Tecnologia FCT/MCTES (PIDDAC) and Centro2020, Grant/Award Number: UIDB/04044/2020 and UIDP/04044/2020; Associate Laboratory ARISE and PAMI, Grant/Award Number: LA/P/0112/2020 and ROTEIRO/0328/2013; Research Unit INESC MN and FCT, Grant/Award Number: UID/05367/2020 and UIDB/50022/2020

Abstract

Aim: This study aimed to experimentally validate a computational fluid dynamics (CFD) model, using micro-particle image velocimetry (micro-PIV) measurements of the irrigation flow velocity field developed in confluent canals during irrigation with a side-vented needle.

Methodology: A microchip with confluent canals, manufactured in polydimethylsiloxane was used in a micro-PIV analysis of the irrigation flow using a side-vented needle placed 3 mm from the end of the confluence of the canals. Velocity fields and profiles were recorded for flow rates of 0.017 and 0.1 ml/s and compared with those predicted in CFD numerical simulations (using a finite volume commercial code – FLUENT) for both laminar and turbulent regimes.

Results: The overall flow pattern, isovelocity and vector maps as well as velocity profiles showed a close agreement between the micro-PIV experimental and CFD predicted data. No relevant differences were observed between the results obtained with the laminar and turbulent flow models used.

Conclusions: Results showed that the laminar CFD modelling is reliable to predict the flow in similar domains.

KEYWORDS

computational fluid dynamics, confluent canals, endodontics, irrigation, micro-particle image velocimetry, positive pressure irrigation

INTRODUCTION

In root canal treatment procedures irrigation plays a key role in cleaning and disinfecting the root canal system space (Haapasalo et al., 2005). The success of the irrigation protocol depends very much on both chemical and mechanical effectiveness, whose importance becomes much more relevant in anatomical regions inaccessible to endodontic instruments (Lee et al., 2004).

Due to the necessity to better understand the real characteristics of the irrigation process, the computational fluid dynamics (CFD) tool has been used to enhance irrigation knowledge, allowing a deeper understanding of the irrigant flow pattern, apical pressure or wall shear force generation within the root canal system space under different conditions such as: irrigation needle design and placement (Boutsioukis, Lambrianidis, Verhaagen, Versluis, Kastrinakis, et al., 2010; Shen et al., 2010; Wang et al., 2015); flow rate (Boutsioukis et al., 2009); or even root canal anatomy (Boutsioukis, Gogos, Verhaagen, Versluis, Kastrinakis, & van der Sluis, 2010a, 2010b; Boutsioukis & Nova, 2021; Loroño et al., 2020). In fact, the use of CFD simulations offers in many cases a huge advantage over experimental tests, where the gathering of similar results would be very difficult or even impossible. Nonetheless, the validity and accuracy of the CFD results are highly dependent on numerous factors and specific settings, which are inputted, into the system, prior to the simulation, when conducting an assessment of a particular problem. In order to determine, and (or) confirm, the most correct and advisable settings, as well as the accuracy of the obtained results, it is recommended to have the CFD outcomes compared with the ones from corresponding laboratorial experimental tests (Versteeg & Malalasekera, 2007).

The micro-particle image velocimetry (micro-PIV) is an experimental measurement technique used to obtain quantitative and qualitative data on the velocity fields of flows, within microfluidic devices, enabling to validate numerical simulations (Calado et al., 2016; Lindken et al., 2009; Silva et al., 2008, 2019). A previously published study (Boutsioukis, Verhaagen, Versluis, Kastrinakis, & van der Sluis, 2010) aimed to compare the CFD simulation outcomes, assuming a non-turbulent flow, with the ones from micro-PIV tests, considering the irrigant flow within a geometrical frustum of a cone during irrigation with a side-vented needle. Not only the agreement between both *in silico* and *in vitro* experimental tests results was good, but the research outcomes and acquired knowledge allowed to gather a data set that was used as reference for validation purposes of CFD results on irrigation works that the authors carried out later (Boutsioukis, Gogos, Verhaagen, Versluis, Kastrinakis, & van der Sluis, 2010a,

2010b; Boutsioukis, Lambrianidis, Verhaagen, Versluis, Kastrinakis, et al., 2010; Boutsioukis & Nova, 2021). Other studies (Gao et al., 2009; Shen et al., 2010) have attempted to validate CFD simulations, considering the existence of turbulence, using the transitional flow shear-stress transport (SST) $k-\omega$ model. The CFD predictions in those studies were qualitatively compared to *in vitro* experimental tests that revealed the absence or presence of a dye solution after irrigation in a plastic block.

Confluent root canals are an anatomic feature that can be present in roots containing a multiple canal system configuration (Versiani et al., 2018). This type of anatomy can lead to a fluid flow different from that observed in single or independent canals. To date, and to the best of the authors' knowledge, no studies using three-dimensional numerical simulations have analysed the irrigant flow dynamics in this type of anatomical configuration.

The aim of the present study is to document the irrigant flow characteristics, such as the velocity vector maps and velocity profiles, in confluent Y-shaped canals during irrigation with a side-vented needle, using micro-PIV, in order to validate a CFD model and the corresponding predictions. These CFD predictions were performed assuming both laminar and turbulent flows (the latter modelled with the SST $k-\omega$ model) with the purpose of assessing the presence or absence of turbulence in the flows studied herein.

MATERIALS AND METHODS

CFD numerical simulation

The geometry and dimensions of the confluent canals were designed in Solidworks software (SolidWorks 2017×64 Edition, Dassault Systèmes), and used for both the CFD simulation and microchip physical manufacture (Figure 1a,b). The canals cross-section was quadrangular, with nominal dimensions of 0.5 mm on each side. The total nominal length was 10 mm, from which the last 3 mm (apical portion) were confluent and independent on the initial 7 mm (coronal portion). The canals were open to the irrigation chamber at the coronal portion and closed at the apical end.

A side-vented needle was modelled in Solidworks software (SolidWorks 2017×64 Edition, Dassault Systèmes), with the dimensions obtained from a scanning electron microscope (Vega3-LMU, TESCAN) micrograph analysis of a 30G side-vented needle (Max-i-Probe, Dentsply/Tulsa Dental). From measurements, the outer diameter was found to be 0.32 ± 0.002 mm and the inner diameter 0.17 ± 0.005 mm. The length of the needle was set to 25 mm. The needle was placed centred into one of the

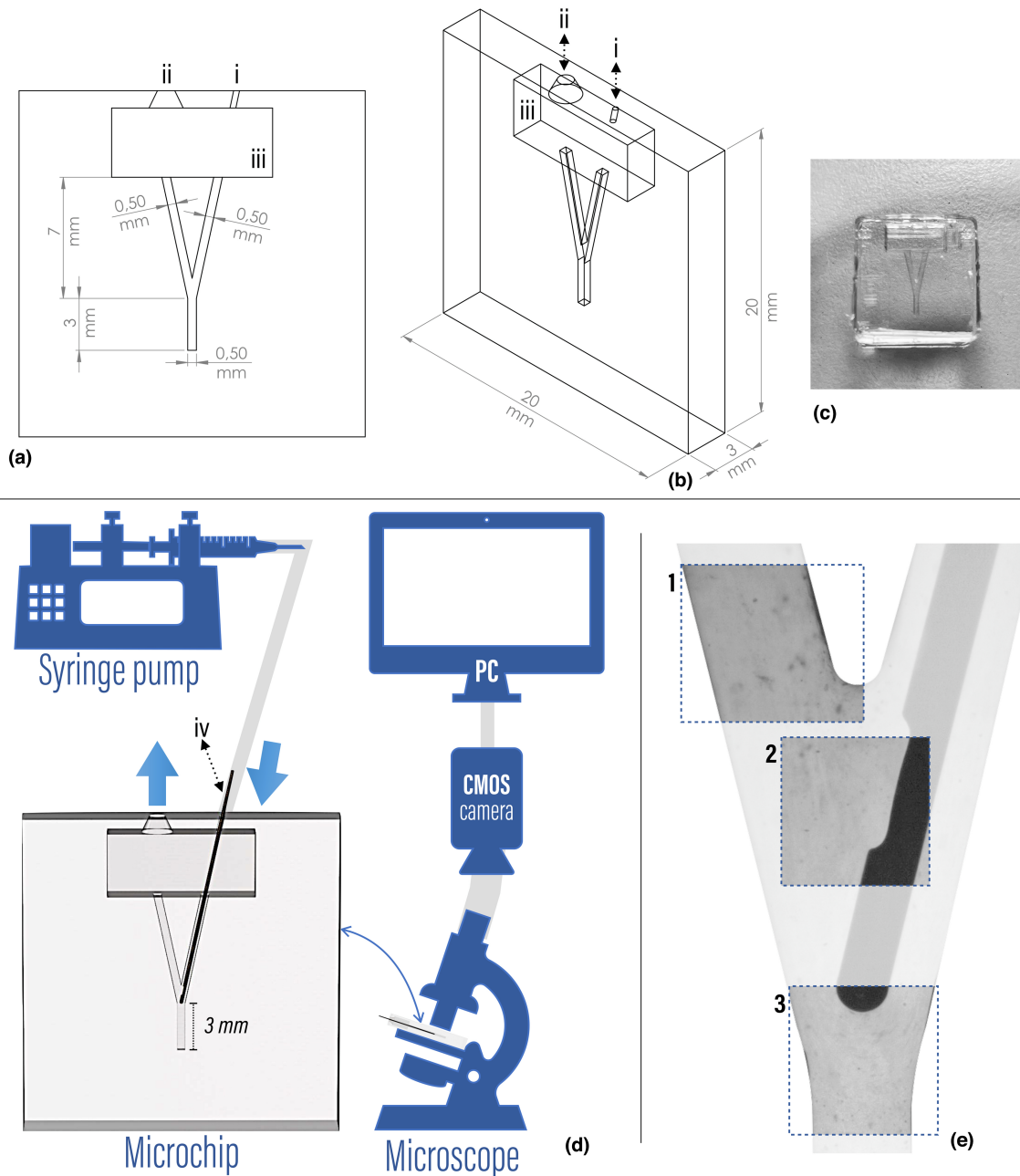


FIGURE 1 CAD drawings and dimensions used for microchip manufacture (a, b), inlet slot for needle placement (i), irrigant outlet (ii) upper chamber for irrigation (iii), microchip manufactured (c). Experimental setup (d). Blue arrows represent inlet, through the needle (iv) and outlet of the irrigant. Regions of interest (e 1–3).

canals so that the tip was positioned 3 mm from its end with the outlet side placed in the two canals confluence area facing the contralateral canal, where the flow pattern was expectedly different from the ones reported within independent canals.

This three-dimensional model was imported into ANSYS 2019 R2 (ANSYS Inc.). After defining the flow domain for the simulation and grid independence tests, a final mesh containing 1 377 874 elements was generated using the ANSYS Workbench meshing pre-processing module. It consists of tetrahedral unstructured meshes

with prism layers in the near-wall region and appropriate near-wall refinement. The numerical modelling of the flow employed the ANSYS Workbench Fluent solver module. A three-dimensional, incompressible, pressure-based transient solver was used.

A velocity inlet boundary condition was applied at the inlet of the needle, with plug velocity profiles matching the inlet flow rates of 0.017 and 0.1 ml/s. For each flow rate, two different dynamical flow models were simulated, laminar and turbulent, the latter resorting to the SST formulation of the $k-\omega$ turbulence model (employing

the coefficients suggested by ANSYS Fluent [ANSYS Inc.] and the Low-Re corrections). The fluid used in the CFD numerical simulations was distilled water, and it was modelled as an incompressible Newtonian fluid with density $\rho = 998 \text{ kg/m}^3$ and viscosity $\mu = 1.0 \times 10^{-3} \text{ Pa}\cdot\text{s}$ (White, 2017). Atmospheric pressure was imposed at both root canal orifices, while canal walls were set as rigid and impermeable surfaces where the no-slip velocity condition applies.

The SIMPLE algorithm was used for pressure–velocity coupling. Second-order discretization schemes were used for the spatial discretization of the velocity and turbulence equations. The convection term used a second-order upwind scheme. The simulations started considering an initial resting state ($u = 0$) and a uniform pressure field ($p = 0$) for the fluid inside the simulation domain. For the time discretization, a bounded second-order implicit discretization formula was used with a $10 \mu\text{s}$ time step for a real flow time of 1 s. The solver stopped for a convergence criterion of 0.001, applied to all simulated flow variables. At the end of the simulations, the ANSYS Workbench CFD-Post module was used to extract the final results and data. A workstation with a 24-core Intel Xeon 2.4 GHz processor (Intel) and internal memory of 128 GB was used for the numerical simulation.

Microchips manufacture

Following the design employed at the CFD simulation the microchips containing the confluent canals were manufactured by soft lithography using polydimethylsiloxane (PDMS, 10:1, 0.5 mm thickness, SYLGARD®184 silicone elastomer, Dow Corning, Midland; Figure 1c) following Silverio and Cardoso de Freitas (2017). The mould used consisted of two parts: lithographed photosensitive resin (100 μm -high, SU-8 50, permanent epoxy negative photoresist, Microchem) to mould the canals and micromilled polymethyl methacrylate (PMMA, 2.20 mm, Perspex®) to mould the inlet for needle placement, (Figure 1a,i) the outlet (Figure 1a,ii) for the irrigant and the chamber for irrigation output (Figure 1a,iii).

Micro-PIV experimental setup and procedure

After manufacture, the microchip was placed under an optical microscope (CX41 UIS2, Olympus Corporation) and a 30G side-vented needle (Max-i-Probe, Dentsply/Tulsa Dental) was placed in the same position as the one used in the CFD simulation. The inlet slot manufactured in the upper chamber of the microchip ensured that the

needle was centred and fixed in this position throughout the experimental test (Figure 1d).

The assembly of devices and materials outlined in Figure 1d consisted of a syringe pump (Nexus N6000, Chemyx Inc.) with a 10 ml disposable syringe (BD) connected to the needle inserted at the inlet of the microchip (Figure 1a,i) through a Luer-lock connector (Merck KGaA). Attached to the microscope, a high-speed and high-resolution monochromatic CMOS camera (CR600x2, Optronis) used to acquire the flow images, through a $\times 4$ magnification objective lens (PlanC N 4 \times ; Olympus) allowed the computer assisted visualization, recording of images and processing of data. The microscope was focused at the centre plane of the canal. The depth of focus of the objective lens was determined to be approximately 118 μm (Meinhart et al., 2000), which represents about one-quarter of the canal depth. As such, the measured velocities represent an average of the flow velocity within this thickness of 118 μm . From the above exposed, a better match between micro-PIV and CFD velocity solutions was found by shifting the CFD measurement plane by approximately $118/2 \approx 60 \mu\text{m}$ from this canal centre region. Illumination was ensured by two independent and continuous cold-light sources. (Olympus KL 1500 LCD, SCHOTT North America, Inc.).

Tracer particles with a diameter of 0.5 μm (Polybead®, Polysciences Inc.) diluted in distilled water with a concentration of 0.75% were used for irrigation. The images were recorded at three different regions of the microchip (Figure 1e), namely at the needle outlet (Figure 1e,2), at the needle tip (Figure 1e,3), and at the start of the artificial canal without needle counting from the confluence (Figure 1e,1). In each region, several sequential images were taken at different frame rates (up to 30 000 frames per second [fps]) to measure the velocities of two irrigant flows with inlet volumetric rates of 0.017 and 0.1 ml/s. The image resolution changed according to the frame rate used (Table 1). Considering the camera pixel size of 14 μm /pixel the minimum area resolved with the $\times 4$ magnification lens was $3.5 \times 3.5 \mu\text{m}^2$. Exposure time was one fifth of the interframe time, leading to 6700 ns on the highest frame rate. With this procedure, it was possible to get a deeper insight and understanding of the generated flows. Nonetheless, the 0.1 ml/s reference value was

TABLE 1 Image resolution according to frame rate

Frame rate (fps)	Resolution (pixel \times pixel)
1250	800 \times 600
6000	256 \times 256
15 000	128 \times 128
30 000	64 \times 64

chosen to match previous published studies (Boutsioukis & Nova, 2021; Loroño et al., 2020) and because it was on the range of realistic values from a clinical point of view (Boutsioukis et al., 2007).

The images were acquired, post-treated and selected through TimeBench software (TimeBench v2.6.30.100, Optronis) before further processing with DynamicStudio software (DynamicStudio v2.0.73, Dantec Dynamics). The use of DynamicStudio allowed image analysis and post-processing to obtain velocity vector maps and

velocity profiles for comparison with CFD numerical simulations.

Data analysis

The data obtained with the micro-PIV and the CFD simulations referring to both laminar and turbulent flow regimes were matched for vector velocity maps, isovelocity maps and three velocity profiles located in the regions of interest.

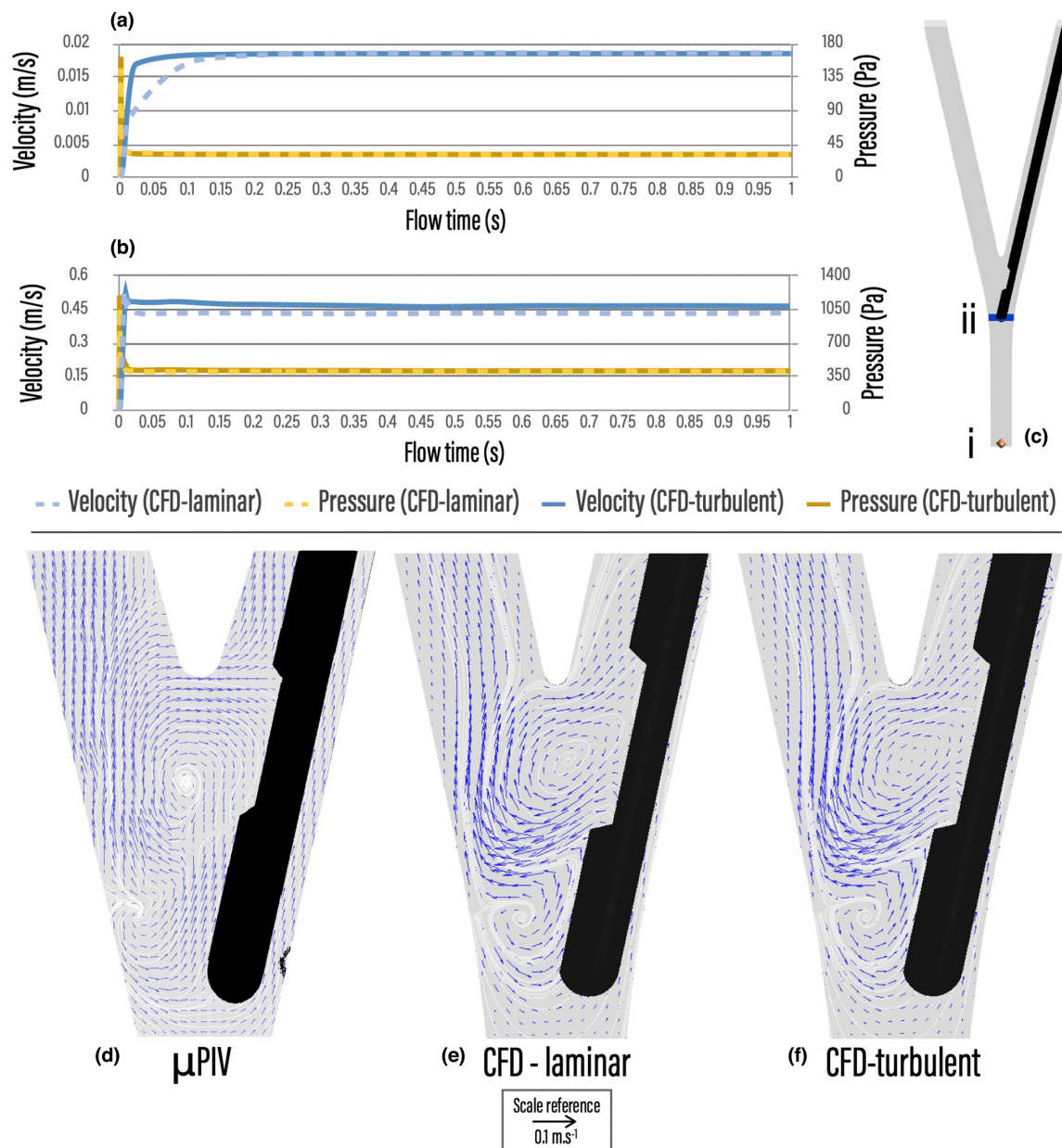


FIGURE 2 CFD results of the velocity and pressure change over time (1 s) for inlet flow rates of 0.017 ml/s (a) and 0.1 ml/s (b). 3D model (c) showing the location where pressure (i) and velocity (ii) were measured to monitor the numerical solution. Overall flow pattern registered in micro-PIV (1250 fps) (d) and predicted in CFD with a laminar (e) and a turbulent model (f) for 0.017 ml/s inlet flow rate. The size of the arrows is coincident with the velocity magnitude.

RESULTS

Micro-PIV and CFD velocity maps characterization

The Figure 2a,b summarizes the velocity and pressure changeover, 1 s simulation time, for 0.017 and 0.1 ml/s, respectively, obtained with CFD simulations with conditions described above. The flow starts from a rest situation, undergoes a short transient period, and stabilizes over a steady-state regime, both for pressure and velocity solutions.

The generated flow patterns depicted in Figure 2d–f were characterized by a jet at the needle outlet, directed diagonally towards the canal wall, at which two vortices formed. One vortex was observed above the needle outlet and most of the flow within this vortex was directed towards the outlet of the canal opposite to the one containing the needle. The other vortex, of smaller strength, was located below the needle outlet and before the needle tip. Here, the flow circumvented the needle tip and headed towards the outlet of the canal with the needle.

This overall flow pattern was captured in micro-PIV experimental tests (Figure 2d), for an inlet flow rate of 0.017 ml/s and a frame rate of 1250 fps. Such experimental results matched the predicted flow patterns of the numerical CFD results (Figure 2e,f). Also, for this 0.017 ml/s flow rate, no turbulent structures were captured through micro-PIV measurements with an acquisition rate of 6000 fps (Figure 3b1–b3). For an inlet flow rate of 0.1 ml/s, the overall flow pattern was preserved, although the definition of the particles paths was less stable. In fact, for this flow

rate, the image frame rate required for an accurate velocity measurement was between 15000 and 30000 fps, but still no turbulent structures were captured (Figure 3c1–c3).

Overall, the velocity results obtained experimentally with the micro-PIV and by CFD simulation, for inlet flow rates of 0.017 and 0.1 ml/s in the three regions, showed a good agreement for both velocity vector patterns and magnitudes, as depicted by the velocity and isovelocity contour maps (Figure 3). No relevant differences were observed between CFD simulated results using laminar or turbulent conditions for the inlet flow rate of 0.017 ml/s. As for 0.1 ml/s there were only a few minor differences in the direction of the vectors, but the overall flow pattern remained similar between both flow models. The present results suggest also that turbulence, if created within these flows, is not self-sustained due to the micro-sized chip canals and associated turbulence dissipation effects. The laminar flow model accurately predicts the flows tested, given that turbulence, if present, plays a negligible role within the range of parameters tested.

Micro-PIV measured and CFD predicted velocity profiles

Velocity profiles were drawn across the positions marked with a pink line in regions 1, 2 and 3 (Figure 4a). Micro-PIV measurements were compared against CFD predictions imposing either laminar or turbulent flow. The highest velocity magnitudes were recorded at the needle outlet for both inlet flow rates studied (0.017 and 0.1 ml/s) and this feature was captured by both laminar and turbulent CFD predictions. Nevertheless, the CFD simulated results for

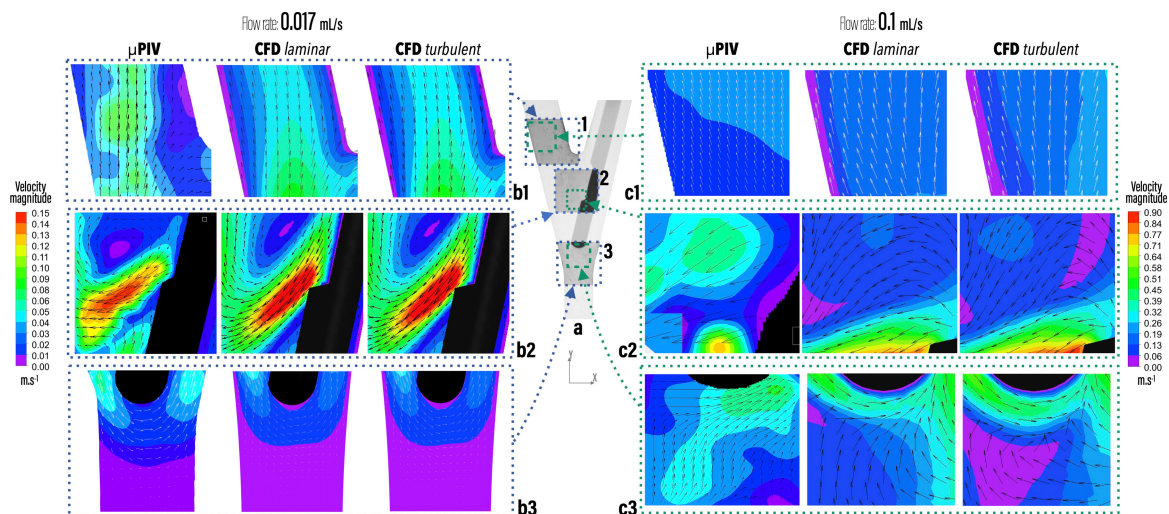


FIGURE 3 Triad of images, for each region, with measured and predicted velocity vectors and isovelocity contour maps, for inlet flow rates of 0.017 ml/s (b1–3) and 0.1 ml/s (c1–3). Micro-PIV images captured with 6000 fps (b1–3), 15000 fps (c1,3) and 30000 fps (c2). The CFD results presented in this section refer to a 1 s simulation time.

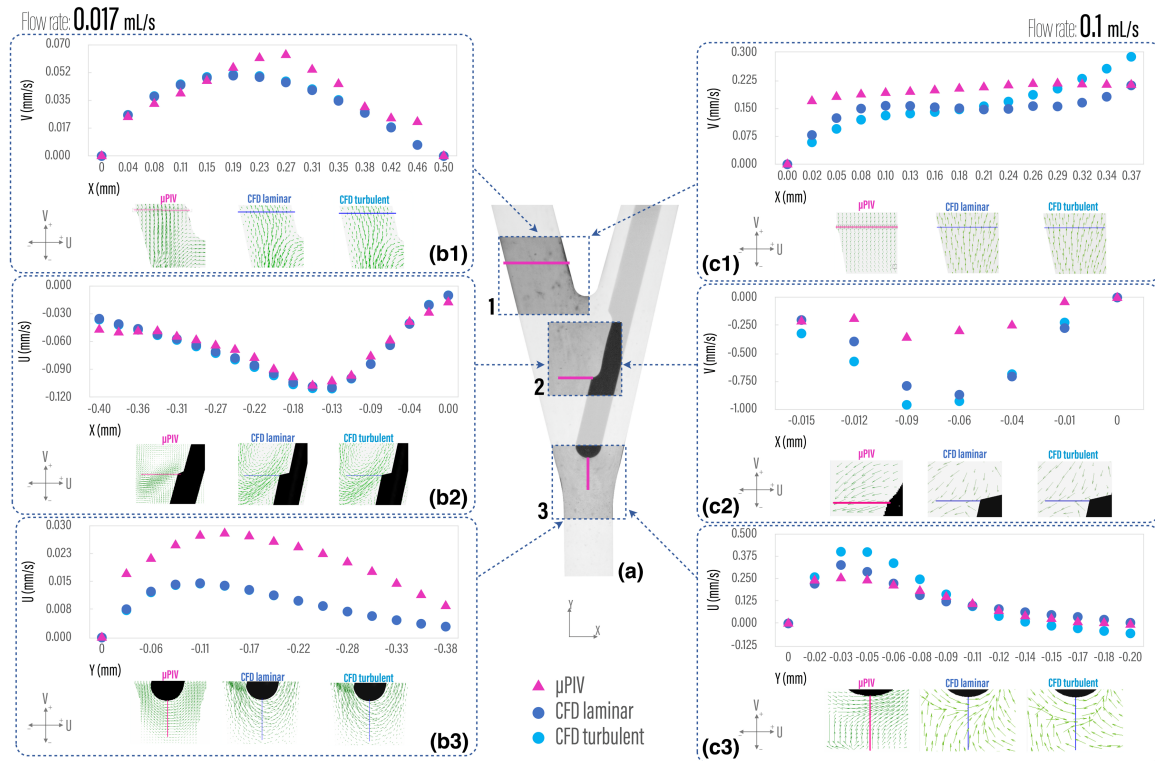


FIGURE 4 Velocity profiles location at region 1, 2 and 3 (a). Measured (μ PIV) and predicted (CFD laminar, CFD turbulent) velocity profiles and vectors for inlet flow rates of 0.017 ml/s (b.1–3) and 0.1 ml/s (c.1–3). Vectors direction are represented with the negative or positive velocities according to the measured component, U or V. Micro-PIV images captured with 6000 fps (b.1–3), 15 000 fps (c.1,3) and 30 000 fps (c.2). The CFD results presented in this section refer to a 1 s simulation time.

laminar conditions describe better the micro-PIV experimental results. Overall, both the magnitude and direction of the velocity components in the traced profiles revealed a good matching.

DISCUSSION

The apical area of the root canal system presents a challenge regarding the efficient and safe delivery of irrigants, mainly under the use of a positive pressure irrigation technique, which has been reported as the most used one among clinicians (Dutner et al., 2012; Willershausen et al., 2015). This challenge has been the subject of previous studies, using numerical simulations analyses, yielding the identification of several factors and their possible influence on a more efficient irrigation and disinfection of this portion of the root canal. Factors related to endodontic procedures such as mechanical preparation size (Boutsioukis, Gogos, Verhaagen, Versluis, Kastrinakis, & van der Sluis, 2010a; Boutsioukis & Nova, 2021) and taper (Boutsioukis, Gogos, Verhaagen, Versluis, Kastrinakis, & van der Sluis, 2010b), needle design (Boutsioukis & Nova, 2021; Boutsioukis, Verhaagen, Versluis, Kastrinakis, Wesselink, & van der Sluis, 2010;

Chen et al., 2014; Loroño et al., 2020; Shen et al., 2010) and its depth of placement (Boutsioukis, Lambrianidis, Verhaagen, Versluis, Kastrinakis, et al., 2010; Boutsioukis & Nova, 2021; Loroño et al., 2020), and fluids flow rate (Boutsioukis et al., 2009) were analysed within a single root canal anatomy. However, the root canal anatomy is another factor that by itself may influence the efficacy of the disinfection at this high clinically relevant apical area. Despite of having been previously addressed and tested by other authors (Wang et al., 2015), the CFD *in silico* simulation has never been validated against corresponding *in vitro* experiments based on velocity for this specific configuration of confluent canals. The present study compares and validates the flow velocity vector maps and profiles inside confluent canals obtained with both micro-PIV experiments and CFD simulations, considering both laminar and turbulent flow regimes. Although the concept is not new, it has never been assessed using this type of canal morphology. This brings to the current study interest and novelty considering the huge impact the root canal configuration may have in the irrigant fluids flow.

The confluent root canals are a type of anatomical configuration, which can be present in multiple roots of the human dentition. Two good examples are the

mandibular molar mesial root, whose percentage of confluent canal may range from 22% to 36%, or the maxillary molar mesiobuccal root with a reported proportion between 18% and 31% (Versiani et al., 2018). In the present study, a simplified geometry of this type of anatomical configuration was used in order to facilitate the achievement of a greater precision in the manufacture of microchips with PDMS and, consequently, a better accuracy in the correspondence with the three-dimensional model used in CFD. Even though this geometry is different from most clinical cases, which usually have a round cross-section, a tapered shape and a lower apical diameter, this geometric simplification was performed herein viewing the purpose of this study – the numerical model validation – and is a standard procedure to reduce errors that could affect the results, as has been discussed in previous works. (Boutsioukis et al., 2022; Oberkamp & Trucano, 2002).

Previous irrigation studies using CFD analysis have shown some differences when comparing the results obtained in terms of generated apical pressure and apical extension of irrigation (Boutsioukis, Gogos, Verhaagen, Versluis, Kastrinakis, & van der Sluis, 2010a, 2010b; Boutsioukis, Lambrianidis, Verhaagen, Versluis, Kastrinakis, et al., 2010; Boutsioukis & Nova, 2021; Gao et al., 2009; Loroño et al., 2020; Shen et al., 2010). One heterogeneity factor among these studies is related to the setup and choice of the flow model. While some authors validated a laminar CFD model, with experimental data acquired with micro-PIV (Boutsioukis, Verhaagen, Versluis, Kastrinakis, & van der Sluis, 2010), which was later employed in several studies (Boutsioukis, Lambrianidis, Verhaagen, Versluis, Kastrinakis, et al., 2010; Boutsioukis & Nova, 2021), others used turbulent modelling in their CFD predictions, with no previous validation based on experimental velocity flow data (Chen et al., 2014; Gao et al., 2009; Loroño et al., 2020; Shen et al., 2010).

As previously mentioned, the optimal settings to obtain the most accurate results with CFD predictions must be obtained through *in vitro* experiments and their yielded data. To the best of the authors' knowledge, only one irrigation study has conducted the validation of the predicted laminar results with CFD simulations against the corresponding measured velocities obtained with the micro-PIV technique (Boutsioukis, Verhaagen, Versluis, Kastrinakis, & van der Sluis, 2010). Two other studies (Gao et al., 2009; Shen et al., 2010) have used a transparent block, with an independent canal, to evaluate the presence or absence of a dye solution after irrigation and compare it with CFD simulations. The experimental results, regarding presence or absence of the dye, have shown a good agreement with the SST $k-\omega$ model, although no quantitative data, regarding velocity or any other physical quantity, were presented.

Despite the large differences in the experimental tests used, none of the above-mentioned studies included both a laminar and a turbulent model to compare with the *in vitro* experimental test. To fill this gap, the present study has included both flow models to assess which one would have a better match with the micro-PIV experiment. The FLUENT commercial code (ANSYS Fluent Theory Guide, ANSYS Inc.) used in the present study to implement and run the CFD simulations offers a multitude of turbulence models (ANSYS, Inc., 2019). Yet, their choice is highly problem dependent. While the $k-\omega$ turbulence model is particularly suited to model the near-wall interactions, which makes it the preferred choice for internal flows, that is flows where the fluid-wall interactions dominate, our problem also features large open flow field regions inside cavities. This type of problem is better described by the SST $k-\omega$ turbulence model, which is a hybrid of $k-\omega$ and $k-\epsilon$ models. That is, it uses the $k-\omega$ model near the walls, transitioning to the $k-\epsilon$ model in the open flow field. As both features coexist in our problem, the SST $k-\omega$ turbulence model seems to guarantee the best compromise between model complexity and accuracy.

Results suggest that, if present, the effect of turbulence is negligible within the range of the tested parameters, namely for flow rates up to 0.1 ml/s. Caution should be taken, however, for future studies using the current validated numerical model with higher flow rates, as they might cause more unsteadiness or even turbulence in the flow. Therefore, prior to using the present CFD code at higher flow rates, additional *in vitro* experiments should be conducted to guarantee the validity of such higher flow rate CFD predictions.

CONCLUSION

The present study showed good agreement between the velocity maps and profiles measured through micro-PIV versus computed CFD. The simplest laminar CFD model used in this study is confirmed to offer reliable results, which can be applied to further studies directed towards evaluating the influence of several clinical parameters on the root canal anatomy presented.

AUTHOR CONTRIBUTION

Mário Rito Pereira: conceptualization, experimental procedures, writing, analysis, review and editing (lead); Goncalo Silva: experimental procedures, writing, analysis, review; Viriato Semiao: experimental procedures, writing, analysis, review; Vania Silverio: experimental procedures, review; Jorge N. R. Martins: writing, analysis, review; Paula Pascoal-Faria: review and editing (supporting); Nuno Alves: review and editing (supporting); Juliana

R. Dias: experimental procedures (supporting); António Ginjeira: review and editing (supporting).

ACKNOWLEDGEMENTS

This work was supported by FCT, through IDMEC, under LAETA, project UIDB/50022/2020. Research Unit INESC MN (UID/05367/2020) acknowledges FCT funding through plurianual BASE and PROGRAMATICO. This research was financially supported by the Fundação para a Ciência e a Tecnologia FCT/MCTES (PIDDAC) and Centro2020 through the following Projects: UIDB/04044/2020; UIDP/04044/2020; Associate Laboratory ARISE LA/P/0112/2020; PAMI – ROTEIRO/0328/2013 (No 022158) and FCT Project Stimuli2BioScaffold, Ref. PTDC/EME-SIS/32554/2017.

CONFLICT OF INTEREST

The authors deny any conflicts of interest.

ETHICS STATEMENT

Not applicable.

DATA AVAILABILITY STATEMENT

Data sharing not applicable

ORCID

Mário Rito Pereira  <https://orcid.org/0000-0002-1632-5809>

Jorge N. R. Martins  <https://orcid.org/0000-0002-6932-2038>

António Ginjeira  <https://orcid.org/0000-0001-5114-1426>

REFERENCES

- ANSYS, Inc. (2019) ANSYS Fluent User's Guide, Release 2019 R2. Canonsburg, PA, USA.
- Boutsioukis, C., Arias-Moliz, M.T. & Chávez de Paz, L.E. (2022) A critical analysis of research methods and experimental models to study irrigants and irrigation systems. *International Endodontic Journal*, 55, 295–329.
- Boutsioukis, C., Gogos, C., Verhaagen, B., Versluis, M., Kastrinakis, E. & van der Sluis, L.W. (2010a) The effect of apical preparation size on irrigant flow in root canals evaluated using an unsteady computational fluid dynamics model. *International Endodontic Journal*, 43, 874–881.
- Boutsioukis, C., Gogos, C., Verhaagen, B., Versluis, M., Kastrinakis, E. & van der Sluis, L.W. (2010b) The effect of root canal taper on the irrigant flow: evaluation using an unsteady Computational Fluid Dynamics model. *International Endodontic Journal*, 43, 909–916.
- Boutsioukis, C., Lambrianidis, T. & Kastrinakis, E. (2009) Irrigant flow within a prepared root canal using various flow rates: a Computational Fluid Dynamics study. *International Endodontic Journal*, 42, 144–155.
- Boutsioukis, C., Lambrianidis, T., Kastrinakis, E. & Bekiaroglou, P. (2007) Measurement of pressure and flow rates during irrigation of a root canal ex vivo with three endodontic needles. *International Endodontic Journal*, 40, 504–513.
- Boutsioukis, C., Lambrianidis, T., Verhaagen, B., Versluis, M., Kastrinakis, E., Wesselink, P.R. et al. (2010) The effect of needle-insertion depth on the irrigant flow in the root canal: evaluation using an unsteady Computational Fluid Dynamics model. *Journal of Endodontics*, 36, 1664–1668.
- Boutsioukis, C. & Nova, P.G. (2021) Syringe irrigation in minimally shaped root canals using three endodontic needles: a Computational Fluid Dynamics study. *Journal of Endodontics*, 47, 1487–1495.
- Boutsioukis, C., Verhaagen, B., Versluis, M., Kastrinakis, E. & van der Sluis, L.W. (2010) Irrigant flow in the root canal: experimental validation of an unsteady Computational Fluid Dynamics model using high-speed imaging. *International Endodontic Journal*, 43, 393–403.
- Boutsioukis, C., Verhaagen, B., Versluis, M., Kastrinakis, E., Wesselink, P.R. & van der Sluis, L.W. (2010) Evaluation of irrigant flow in the root canal using different needle types by an unsteady Computational Fluid Dynamics model. *Journal of Endodontics*, 36, 875–879.
- Calado, B., Santos, A. & Semiao, V. (2016) Characterization of the mixing regimes of Newtonian fluid flows in asymmetrical T-shaped micromixers. *Experimental Thermal and Fluid Science*, 72, 218–227.
- Chen, J.E., Nurbakhsh, B., Layton, G., Bussmann, M. & Kishen, A. (2014) Irrigation dynamics associated with positive pressure, apical negative pressure and passive ultrasonic irrigations: A Computational Fluid Dynamics analysis. *Australian Endodontic Journal*, 40, 54–60.
- Dutner, J., Mines, P. & Anderson, A. (2012) Irrigation trends among American Association of Endodontists members: A web-based survey. *Journal of Endodontics*, 38, 37–40.
- Gao, Y., Haapasalo, M., Shen, Y., Wu, H., Li, B., Ruse, N.D. et al. (2009) Development and validation of a three-dimensional Computational Fluid Dynamics model of root canal irrigation. *Journal of Endodontics*, 35, 1282–1287.
- Haapasalo, M., Endal, U., Zandi, H. & Coil, J.M. (2005) Eradication of endodontic infection by instrumentation and irrigation solutions. *Endodontic Topics*, 10, 77–102.
- Lee, S.-J., Wu, M.-K. & Wesselink, P. (2004) The effectiveness of syringe irrigation and ultrasonics to remove debris from simulated irregularities within prepared root canal walls. *International Endodontic Journal*, 37, 672–678.
- Lindken, R., Rossi, M., Große, S. & Westerweel, J. (2009) Micro-particle image velocimetry (μ PIV): recent developments, applications, and guidelines. *Lab on a Chip*, 9, 2551–2567.
- Loroño, G., Zaldivar, J.R., Arias, A., Cisneros, R., Dorado, S. & Jimenez-Octavio, J.R. (2020) Positive and negative pressure irrigation in oval root canals with apical ramifications: a computational fluid dynamics evaluation in micro-CT scanned real teeth. *International Endodontic Journal*, 53, 671–679.
- Meinhart, C.D., Wereley, S.T. & Gray, M.H.B. (2000) Volume illumination for two-dimensional particle image velocimetry. *Measurement Science and Technology*, 11, 809–814.
- Oberkampf, W.L. & Trucano, T.G. (2002) Verification and validation in computational fluid dynamics. *Progress in Aerospace Sciences*, 38, 209–272.

- Shen, Y., Gao, Y., Qian, W., Ruse, N.D., Zhou, X., Wu, H. et al. (2010) Three-dimensional numeric simulation of root canal irrigant flow with different irrigation needles. *Journal of Endodontics*, 36, 884–889.
- Silva, G., Leal, N. & Semiao, V. (2008) Micro-PIV and CFD characterization of flows in a microchannel: Velocity profiles, surface roughness and Poiseuille numbers. *International Journal of Heat and Fluid Flow*, 29, 1211–1220.
- Silva, G., Semiao, V. & Reis, N. (2019) Rotating microchannel flow velocity measurements using the stationary micro-PIV technique with application to lab-on-a-CD devices. *Flow Measurement and Instrumentation*, 67, 153–165.
- Silverio, V. & Cardoso de Freitas, S. (2017) Microfabrication techniques for microfluidic devices. In: Galindo-Rosales, F.J. (Ed.) *Complex fluid-flows in microfluidics*. Cham, Switzerland: Springer, pp. 25–51.
- Versiani, M.A., Pereira, M.R., Pécora, J.D. & Sousa-Neto, M.D. (2018) Root canal anatomy of maxillary and mandibular teeth. In: Versiani, M.A., Basrani, B. & Sousa-Neto, M.D. (Eds.) *The root canal anatomy in permanent dentition*. Cham, Switzerland: Springer, pp. 181–239.
- Versteeg, H.K. & Malalasekera, W. (2007) *An introduction to computational fluid dynamics: the finite volume method*, 2nd edition. UK: Pearson Education Limited.
- Wang, R., Shen, Y., Ma, J., Huang, D., Zhou, X., Gao, Y. et al. (2015) Evaluation of the effect of needle position on irrigant flow in the C-shaped root canal using a computational fluid dynamics model. *Journal of Endodontics*, 41, 931–936.
- White, F.M. (2017) *Fluid mechanics*, 8th edition. New Delhi, India: Mcgraw-Hill Education.
- Willershausen, I., Wolf, T.G., Schmidtman, I., Berger, C., Ehlers, V., Willershausen, B. et al. (2015) Survey of root canal irrigating solutions used in dental practices within Germany. *International Endodontic Journal*, 48, 654–660.

How to cite this article: Rito Pereira, M., Silva, G., Semiao, V., Silverio, V., Martins, J.N.R. & Pascoal-Faria, P. et al. (2022) Experimental validation of a computational fluid dynamics model using micro-particle image velocimetry of the irrigation flow in confluent canals. *International Endodontic Journal*, 00, 1–10. Available from: <https://doi.org/10.1111/iej.13827>